Geofísica Internacional (2025) **64-1**: 1437 - 1454

Hydraulic permeability prediction from attenuation in an oil well using the squirt flow model

Joseline Mena-Negrete*[1], Raúl del Valle García[3] and Enrique Coconi-Morales[1, 2]

Abstract

A practical methodology is presented for estimating the hydraulic permeability from the wave attenuation at sonic frequencies using the poroelastic squirt flow model associated with the mechanism that encompasses the interaction between solid and fluid in an oil well. The methodology consists of four stages: a) the petrophysical evaluation, b) the static rock physics modeling that includes its diagnostics, c) the estimation of wave attenuations using an inversion scheme to optimize the Z critical parameter from the squirt flow model, d) the correlation between attenuations and the Z parameter with hydraulic permeabilities obtained by conventional well logs and available core analysis. The correlations are the means to establish the predicted hydraulic permeabilities from sonic and ultrasonic data. The obtained results suggest that the Z parameter is low while attenuations are high when the medium presents high porosity and permeability. In the methodology, the inversion scheme is proposed to find the Z parameter, the velocity dispersion, and attenuations in terms of the inverse quality factors, respectively for P-wave (Q_P^{-1}) and S-wave S (Q_S^{-1}) using a simulated annealing technique. The results from the application of the methodology are validated with core data (water saturation, porosity, and permeability) and mineralogical analysis from thin sections by the point counting technique. This methodology promises a means for predicting the hydraulic permeability from sonic and ultrasonic velocities in a well.

Key words: Squirt flow, velocity dispersion, attenuation, permeability.

Resumen

Se presenta una metodología práctica para estimar la permeabilidad hidráulica a partir de la atenuación de ondas a frecuencias sónicas utilizando el modelo poroelástico de flujo squirt asociado al mecanismo que engloba la interacción entre un sólido y un fluido en un pozo petrolero. La metodología consta de cuatro etapas: a) la evaluación petrofísica, b) el modelado de física de rocas estático que incluye su diagnóstico, c) la estimación de atenuaciones de ondas usando un esquema de inversión para optimizar el parámetro crítico Z del modelo de flujo squirt, d) la correlación entre las atenuaciones y el parámetro Z con las permeabilidades hidráulicas obtenidas mediante registros de pozos convencionales y análisis de núcleos disponibles. Las correlaciones son el medio para establecer la predicción de permeabilidades hidráulicas a partir de datos sónicos y ultrasónicos. Los resultados obtenidos sugieren que el parámetro Z es bajo mientras que las atenuaciones son altas cuando el medio presenta alta porosidad y permeabilidad. En la metodología, se propone el esquema de inversión para encontrar el parámetro Z, la dispersión de la velocidad y las atenuaciones en términos de los de los factores de calidad inversos, respectivamente para las ondas, P (Q_P^{-1}) y S (Q_S^{-1}) utilizando la técnica de recocido simulado. Los resultados de la aplicación de la metodología son validados con datos de núcleos (saturación de agua, porosidad y permeabilidad) y el análisis mineralógico de secciones delgadas mediante la técnica de conteo de puntos. Esta metodología promete un medio para predecir la permeabilidad hidráulica a partir de velocidades sónicas y ultrasónicas en un pozo.

Palabras clave: Flujo squirt, dispersión de velocidad, atenuación, permeabilidad.

Received: April 24, 2023; Accepted: September 2, 2024; Published on-line: January 1, 2025.

Editorial responsibility: Dr. Celestino Valle Molina

* Corresponding author: Joseline Mena-Negrete, jmenan@ipn.mx.
[1] Instituto Politécnico Nacional, ESIA, Unidad Ticomán. México City, México
[2] Instituto Mexicano del Petróleo. México City, México
[3] Independent Consultant, Applied Geophysics, Mexico City, Mexico

Joseline Mena-Negrete, Raúl del Valle García, Enrique Coconi-Morales
https://doi.org/10.22201/igeof.2954436xe.2025.64.1.1801

1. Introduction

The permeability (k) is one of the most heterogeneous petrophysical properties in rocks. This property depends on textural and geological factors, such as sorting, diagenesis, grain shape, tortuosity, pore-structure, porosity, fluid saturation, and rock wettability (Nolen-Hoeksema, 2014). k has been determined from core sample tests, geophysical well log data, pressure-transit analysis, production tests, production-history data, and wireline formation testers. The latter considers modern tools such as dual packer and mini-drillstem tests for measuring vertical and horizontal permeability in heterogeneous formations (Ayan *et al.*, 2001). However, there is a high variability of permeability values with different methods, showing that several factors are interlaced, preventing a proper value of hydraulic permeability.

Regarding well logs data, k can be estimated by empirical equations such as Timur, Willye and Rose, Kozeny and Carman from the irreducible water saturation parameter (Tiab and Donaldson, 2004), which can be obtained from Nuclear Magnetic Resonance well logging (NMR). The Stoneley wave was employed to detect changes in permeability to understand fluid flow and electrofacies method to evaluate the reservoir quality, this permeability estimation presented similar results with core permeability and Timur method (Soleimani *et al.*, 2018).

According to Müller *et al.*, (2010), it is inferred that it is possible to estimate hydraulic permeability in oil reservoirs from wave attenuation and velocity dispersion of seismic data. They have been acknowledged three basic types of mechanisms according to a certain frequency range:1) global flow or macroscopic scale model, based on the Biot theory of poroelasticity, 2) squirt or local flow model, and 3) mesoscopic flow model. The global flow mechanism applies at frequencies larger than 100kHz (Müller *et al.*, 2010), the squirt flow works from intermediate frequencies (Mavko *et al.*, 2009), and the mesoscopic model is consistent for seismic exploration frequencies (Pride *et al.*, 2004). Müller *et al.*, (2010) reviewed models for wave attenuation and velocity dispersion based on poroelasticity and viscoelasticity theory by wave-induced fluid flow between heterogeneities of different scales. They showed diverse models in which aspects such as applicability, validity range, and experimental verification remain a big challenge.

The squirt flow model was applied, considering the contact between grains and a spectrum of pore aspect ratios to estimate the wave attenuation, which is negligible for the contact of spherical grains of the same size (Palmer and Traviolia, 1980).

Shapiro and Müller (1999) analyzed that seismic permeability may differ from hydraulic permeability through poroelastic layers with partial saturation at low frequencies. Indeed, Pride *et al.*, (2004) introduced that it is possible to extract permeability information from the attenuation measured at exploration seismic frequencies (1-10^4 Hz).

Some researchers consider that the attenuation by the squirt flow mechanism could be related to permeability. Akbar *et al.*, (1993) analyzed the pore orientation and its effect on P-wave attenuation based on the squirt flow mechanism related to the permeability of sandstone samples. Dvorkin and Nur *et al.*, (1993) introduced the BISQ model, which combines Biot and squirt flow mechanisms to obtain P-wave velocity and inverse quality factor (Q_P^{-1}). Dvorkin *et al.*, (1994) used BISQ indicating that (Q_P^{-1}) is low when the permeability is small and increases to a maximum at intermediate permeabilities.

The main objective of this study is to appraise the proposed methodology to predict the hydraulic permeability from the inverse quality factors obtained by the squirt flow mechanism using available well log data and core velocities. The paper is organized in the following manner. The model used and the methodology are shown in Section 2. The case study and geological framework of an oil well are presented in Section 3. Section 4 focuses on predicting hydraulic permeability from the petrophysical evaluation, the rock physics modeling, as well as the estimation of inverse quality factors, including the Z parameter, using an inversion scheme based on the squirt flow model. Finally, a correlation is established between inverse quality factors and the Z parameter with the hydraulic permeability from the core and the well log data. This paper closes with a discussion of the limitations encountered and the needed considerations for future contributions.

2. Models review and methodology

2.1 Squirt flow model

The squirt flow or local flow indicates that when elastic waves propagate in an isotropic and homogeneous rock, pore pressure gradients are created, causing a local fluid flow inside the pores. These effects are incorporated on the macroscopic scale of grains and pores (Dvorkin *et al.*, 1994).

Mavko and Jizba (1991) included the effect of local flow to estimate unrelaxed velocities at high pressure and frequency. Dvorkin *et al.*, (1995) considers that the rock porosity includes soft and stiff pores. When the waves propagate, the soft pores transfer more stress to the fluid than the stiff pores, and this induces pore pressure, which is equilibrated at low frequency by Gassmann (1951). In the intermediate frequencies, there is a flow between stiff and soft pores; this produces energy dissipation and, therefore, velocity dispersion and attenuation. When the fluid is unrelaxed, it impedes the flow between pores at very

high frequencies. The attenuation reaches zero. However, in the squirt or local flow, there is a modified solid that includes the soft pores, and the modified frame has rock porosity corresponding to stiff pores. Therefore, squirt flow describes the interaction between the matrix and the fluid inside the pores in the rock.

Dvorkin *et al.*, (1995) extended the squirt flow mechanism by Mavko and Jizba (1991) to estimate velocity dispersion and inverse quality factors for low and high frequencies employing the complex bulk elastic modulus of the saturated rock (K_r) that is given by:

$$K_r = \frac{K_{\mathrm{m}}}{1-\alpha_{\mathrm{m}} dP / d\sigma} \tag{1}$$

Where K_m is the bulk modulus of the modified solid, $\alpha_{\mathrm{m}}=1-K_{\mathrm{m}}/K_{\mathrm{ms}}$, K_{ms} is the bulk modulus of the saturated modified solid, and $dP/d\sigma$ is the ratio between pore pressure and hydrostatic confining stress (Appendix A).

The complex shear modulus of the modified solid (μ_m) is given by:

$$\mu_m = \left[\frac{1}{\mu_{dry}} - \frac{4}{15}\left(\frac{1}{K_{\mathrm{dry}}} - \frac{1}{K_{\mathrm{md}}} \right) \right]^{-1}, \tag{2}$$

where μ_{dry} and K_{dry} are the dry shear modulus and the dry bulk modulus, respectively. K_{md} is the dry bulk modulus modified (See Appendix A).

The complex compressional modulus (M_m) is calculated from:

$$M_m = K_r + {}^{4}\!/_{3}\mu_m \tag{3}$$

The compressional (V_{P}) and shear wave (V_{S}) velocities consider the real part of M_m and μ_m, correspondingly:

$$V_p = \sqrt{\frac{Re(M_m)}{\rho_{sat}}},\ V_s = \sqrt{\frac{Re(\mu_m)}{\rho_{sat}}}, \tag{4}$$

where ρ_{sat} is the saturated density.

The inverse quality factors of P-wave (Q_{P}^{-1}) and S-wave (Q_{S}^{-1}) are the ratio of the real and the imaginary part of M_m and μ_m, respectively. The Q_{P}^{-1} and Q_{S}^{-1} are given by:

$$Q_{\mathrm{P}}^{-1} = \left| \frac{\mathrm{Im}(M_m)}{\mathrm{Re}(M_m)} \right|,\ Q_S^{-1} = \left| \frac{\mathrm{Im}(\mu_m)}{\mathrm{Re}(\mu_m)} \right| \tag{5}$$

Dvorkin *et al.*, (1995) introduced the Z parameter which is the ratio of characteristic squirt flow length (R) and the diffusivity of the soft pore (k):

$$Z = \sqrt{\frac{R^2}{\mathrm{k}}}, \tag{6}$$

R is a parameter that represents the radial flow of fluid inside pores with grains (Murphy *et al.*, 1986), not depending on the frequency. Finding Z is matching the measured velocities with predicted velocities by the squirt flow model. Figure 1 presents the squirt flow mechanism due to the elastic wave propagation from a sonic tool in a well.

2.2 Methodology

The proposed methodology consists of four stages (Figure 2). The first stage is the petrophysical evaluation, where properties such as total porosity (PHIT), effective porosity (PHIE), water saturation (S_{w}), hydraulic permeability, and mineralogy are estimated from density (RHOB), neutron (NPHI), resistivity, and sonic well logs.

The second stage is the rock physics modeling, which comprises two steps; bringing the interval to be examined to a common fluid denominator and finding a model that matches and explains well log data through velocity-porosity relationship (Dvorkin *et al.*, 2014). The squirt flow model requires the effective dry rock elastic moduli (K_{dry}) obtained from the static rock physics modeling.

The third stage is the inversion for obtaining Z, dispersion of velocities and inverse quality factors (Q_{P}^{-1}, Q_{S}^{-1}). Here, the simulated annealing approach was used for solving the objective function given by:

$$\begin{aligned} OF(Z) = {} & w_1(\mathrm{V_P}(0.5\,\mathrm{MHz}) - \mathrm{V_{P\text{-}ult}})^2 + w_2(\mathrm{V_S}(0.5\,\mathrm{MHz}) - \mathrm{V_{S\text{-}ult}})^2 \\ & + w_3(\mathrm{V_P}(10\,\mathrm{kHz}) - \mathrm{V_{P\text{-}log}})^2 + w_4(\mathrm{V_S}(10\,\mathrm{kHz}) - \mathrm{V_{S\text{-}log}})^2, \end{aligned} \tag{7}$$

where $\mathrm{V_{P\text{-}log}}$ and $\mathrm{V_{S\text{-}log}}$ are the measured P-wave and S-wave velocities from well logs. $\mathrm{V_{P\text{-}ult}}$ and $\mathrm{V_{S\text{-}ult}}$ are the P-wave and S-wave velocities estimated from core velocities. $\mathrm{V_P}$ (0.5 MHz,10 KHz) and $\mathrm{V_S}$(0.5 MHz,10 KHz) are the predicted P-wave and S-wave velocities by the squirt model at these frequencies. w_{i}, where subscript i=1-4 indicates the weighting factors to velocities, respectively.

The fourth stage corresponds to establish the correlation between the hydraulic permeability with the Z parameter and attenuations in terms of inverse quality factors. This correlation

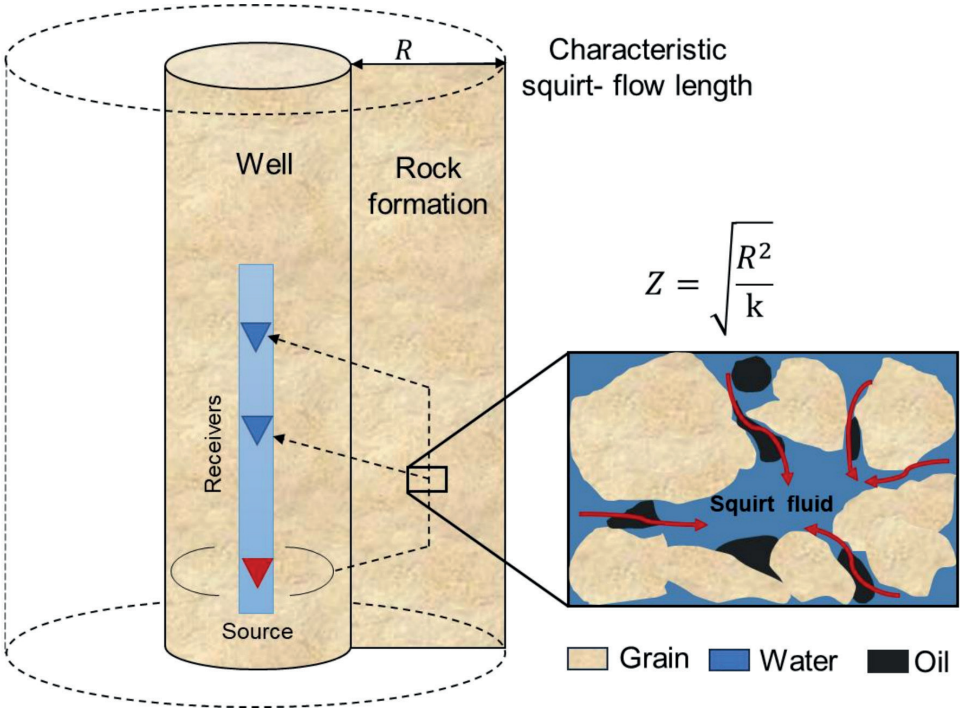

Figure 1. Schematic diagram of squirt or local model applied in an oil well (modified from Dvorkin *et al.*, 1995).

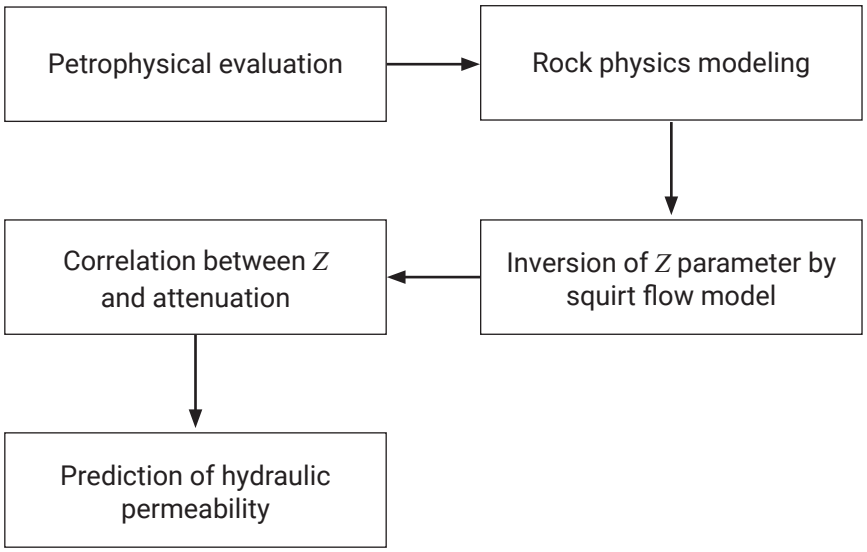

Figure 2. The general methodology is divided into four stages. The first is the petrophysical evaluation, then is the rock physics modeling. The inversion scheme to find parameters (*Z*, dispersion of velocities and inverse quality factors) by the squirt flow model in the third stage. Finally, the correlation between hydraulic permeability with the *Z* parameter and inverse quality factors is considered with another property to predict hydraulic permeability.

also could be calculated in terms of another property. Finally, the correlation function is applied to predict hydraulic permeability.

3. Case study

The open database available from the Volve field by Equinor from June 2018 is used in this work. This database is subject to an Equinor Open Data License of September 2020. Well log and core data, thin section information, PVT analysis, and reports corresponding to the oil well 15/9–19A were used.

The Hugin formation of well 15/9–19A corresponds to the Upper Jurassic (Middle Callovian to Middle Oxfordian) is analyzed. The core sampling report indicates a sandstone formation with fine to coarse grains, subangular to sub-rounded, friable to firm with small amounts of clay, calcareous, and silica cement (Østby*et al.*, 1998).

The Hugin formation comprises a mixture of minerals like quartz, clay, mica, calcite, coal, feldspar, and pyrite (Ringheim, 1999). According to Vollset and Dore (1984), the Hugin formation was exposed to meteoric water that contributed to the dissolution of minerals. Evidence of diagenetic processes has been studied in the well, such as stylolites generated by dissolution during compaction, quartz and calcite cementation, kaolinitization and illitization. These last processes are interrelated with alkali feldspar and kaolinite decomposition to form illite (Lunde, 2013).

The thin section at different depths shows quartz grains with calcite cement (Figure 3a), and the quartz grains become rounded with varying degrees of consolidation (Figure 3b and c). Stylolites also exist between the quartz grains and feldspar (Figure 3d).

4. Results of applying the four stages' methodology

The application of the methodology (Figure2) in the well 15/9–19A is shown in this section. It starts with the petrophysical evaluation results (Section 4.1). The rock physics modeling is

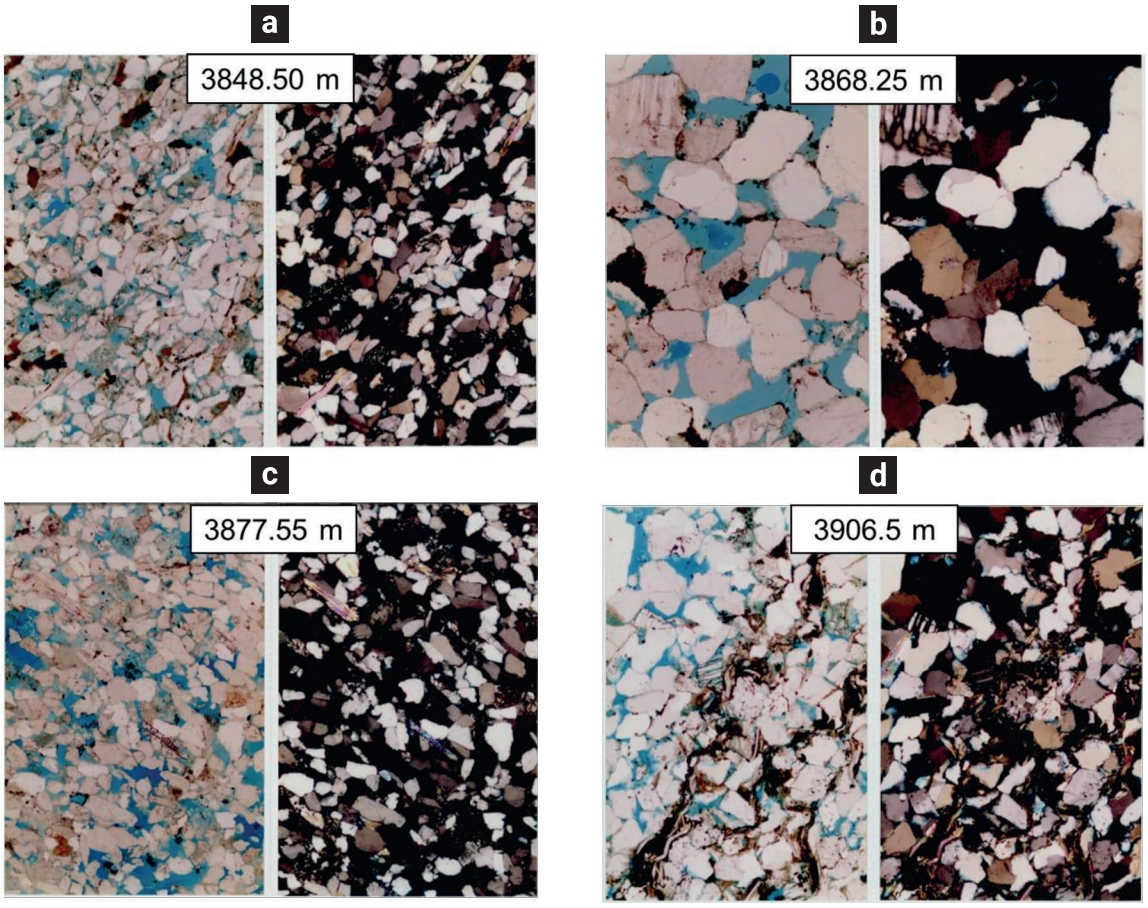

Figure 3. Thin sections of well 15/9–19A at different depths, a) 3848.5 m, b) 3668.25 m, c) 3876.55 m, and d) 3906.5 m taken from Statoil (1998a). The figures on the left have plane-polarized light, and those on the right have cross-polarized light.

presented in Section 4.2. The inverse scheme to find parameters from the squirt model is shown in Section 4.3. Finally, Section 4.4 includes the correlations of the hydraulic permeability with inversion results and the prediction of hydraulic permeability in the well.

4.1 Petrophysical evaluation

The results of the petrophysical evaluation of Hugin formation in the well 15/9–19A indicate high oil saturation and high total porosity (PHIT). The mineral content is quartz, feldspar, mica, calcite, and clay. The permeability varies between 200 and 20000 mD (Figure 4). The information reported by Lunde (2013) revealed that this well shows the presence of quartz cement; however, it was not possible to estimate it with the well log data available. The calcite cement is considered from thin sections (Figure 3) and the response of well logs, because of the density well log (RHOB) increases up to a 2.71 g/cm^3, PHIT decreases between 3 and 10 %, and permeability also decreases in areas with a higher percentage of calcite. In general, the clay volume is low, which can be structural as it presents processes of replacement of quartz grains due to diagenetic processes (Lunde, 2013).

Three types of facies were identified from neutron porosity (NPHI), density (RHOB), compressional (DTC), and shear transit time (DTS) logs. The first facies is sandstone that varies in consolidation degrees; the second and third correspond to sandstone with a lower and higher degree of calcite cement, respectively (Figure 4, track 8). Based on the description of core plugs reported by Ringheim (1999), at 3849 m it is observed a light grey fine-grained sandstone with mica, and at 3868 m the sandstone shows small stylolites that may be filled with organic matter; this has a lower degree of consolidation than the previous one. The plug at 3899 m is composed of consolidated sandstone. Finally, the plug at 3911 m contains fine-grained sandstone, well consolidated with higher mica content (Figure 4, track 11).

It is important to note that in the depth range of 3877-3880 m, the resistivity and transit time logs show an altered zone, probably due to drilling fluid. Therefore, this depth range was not interpreted (poor quality data in Figure 4).

The mineralogic volume in Figure 4, Track 9 was calibrated with the mineralogy reported by Ringheim (1999) through the point-counting analysis performed on thin sections. There is evidence that the resolution between the scale of thin sections and well logs is different; however, it was used to identify the mineral trend (Figure 5b-e). On the other hand, Figure 5a shows the effective porosity (PHIE) estimated by removing the clay content from the total porosity, showing a match with the effective porosity measured from core analysis (measurements in the centrifuge) reported by Ringheim.

4.2 Rock physics modeling

The soft-sand and Differential Effective Medium (DEM) models were used to show which model best explains the Hugin formation through the velocity-porosity relationship. It should be noted that these models were also applied to estimate the dry rock bulk modulus (K_{dry}) which is an essential parameter to apply the squirt flow model.

According to the point-counting analysis reported by Ringheim (1999), the Hugin formation shows kaolinite and a mixture of clays, feldspar as alkali feldspar, plagioclase, or albite, and mica as biotite, and muscovite. Given there is a variety of different clay, feldspar and mica minerals, the Voigt-Reuss-Hill average was applied in each case. Where the elastic moduli of mixed of those minerals are shown in Table 1.

4.2.1 Soft-sand model applied to Hugin formation

The soft-sand contact model combines the Hertz-Mindlin model and the modified Hashin-Shtrikman lower bound to calculate the dry elastic moduli of a pack of spherical grains (Dvorkin and Nur,1996). The Hertz-Mindlin model (Mindlin, 1949) requires the correction for friction coefficient (f) in the shear modulus. This coefficient is related to the tangential forces due to oscillatory stress when waves propagate in the rocks (Mavko *et al.*, 2009). The Poisson's ratio of the grain material (v_m) and the Poisson's ratio of the grain pack (v_p) need to be known to calculate f; the former is estimated from the Voigt-Reuss-Hill average of minerals and the corresponding elastic moduli; the latter is obtained from saturated well logs by applying the Gassmann fluid substitution (1951) to estimate K_{dry} and $\mu_{dry} = V_S^2 \rho_{sat}$ .Where V_s is the shear wave velocity. Once the Poisson ratios, v_m and v_p are known, the friction coefficient is calculated.

According to the friction coefficient, when $f=0$, all the grains slip, while $f=1$ implies no slip between grains (Mavko *et al.*, 2009). Figure 6 shows the friction coefficient results. $f=0.25$ was selected to correct the shear modulus in the Hertz-Mindlin model in the Hugin formation (Figure 7). The lightly cemented sandstone shows higher values of the Poisson's ratio of grain material than the unconsolidated sandstone. However, for highly-cemented sandstone, some values of the Poisson's ratio of the grain pack are higher ($0.25<v_p$), it means that the model is not representative of complex sandstones or sandstones with higher calcite volume.

Rock velocities under a fully saturated state have been calculated beyond the dry elastic moduli by the soft-sand model with the Gassmann equations. The velocity-porosity plot of the Hugin formation indicates that it is an unconsolidated formation since it shows high porosity and a low coordination number (n=2-3). Sandstone with lightly-cemented sandstone has values between 2

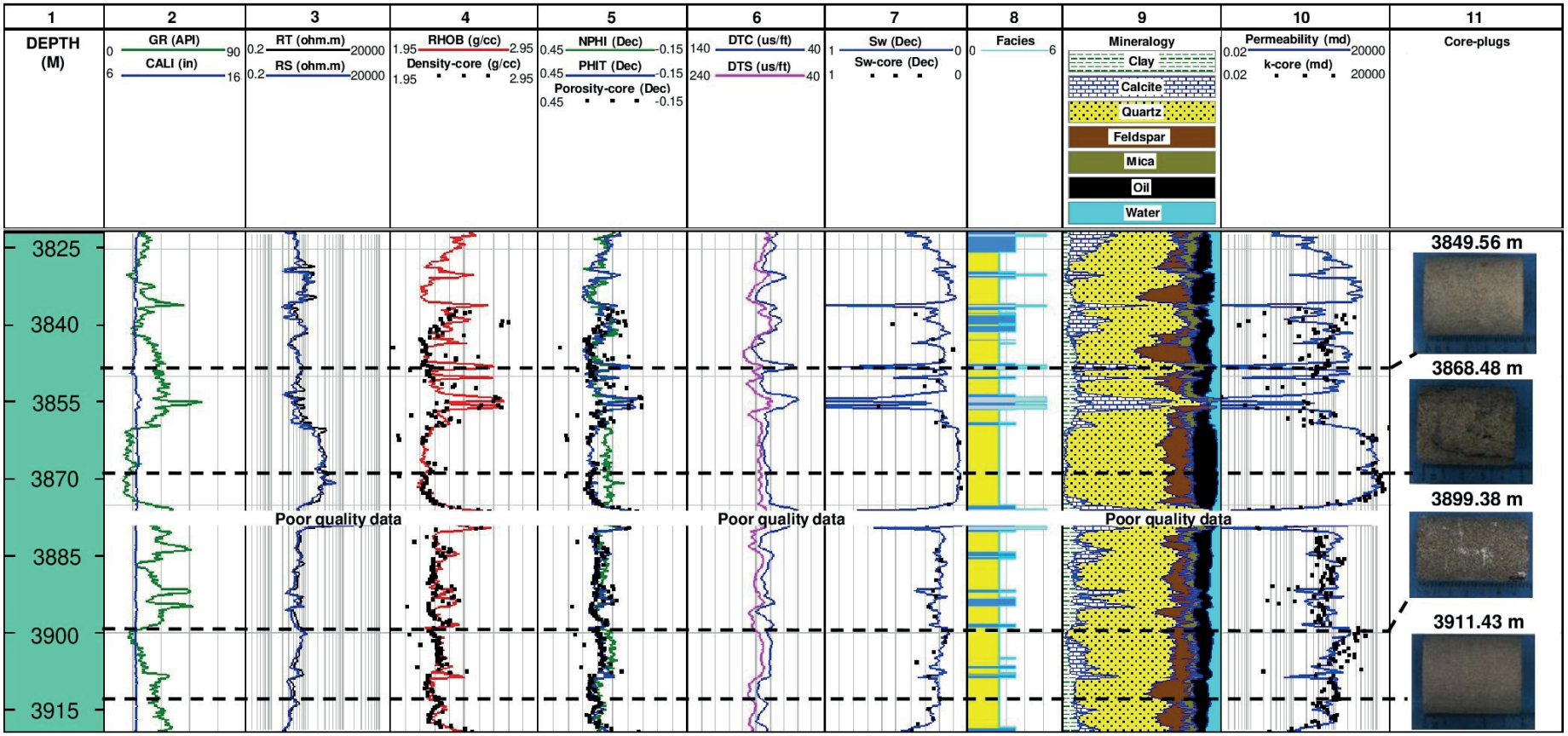

Figure 4. Petrophysical evaluation of Hugin formation in well 15/9–19A. Gamma Ray log (Track 2), Deep (RT), and shallow resistivity (RS) logs (Track 3). Density log (RHOB) and core density (Track 4), neutron porosity log (NPHI), estimated total porosity (PHIT), and core porosity (Track 5). Compressional (DTC) and shear transit time (DTS) logs (Track 6). Estimated water saturation (S_w) and core water saturation ($S_{w\text{-core}}$)(Track 7). In the facies track (Track 8), yellow indicates sandstone, blue and gray represent lightly and highly cemented sandstone, respectively. Mineralogy (Track 9). Estimated permeability by Timur and core permeability (k_{core})(Track 10), and core plugs (Track 11) at different depths taken from Ringheim (1999). Byberg (1998) reported the core properties.

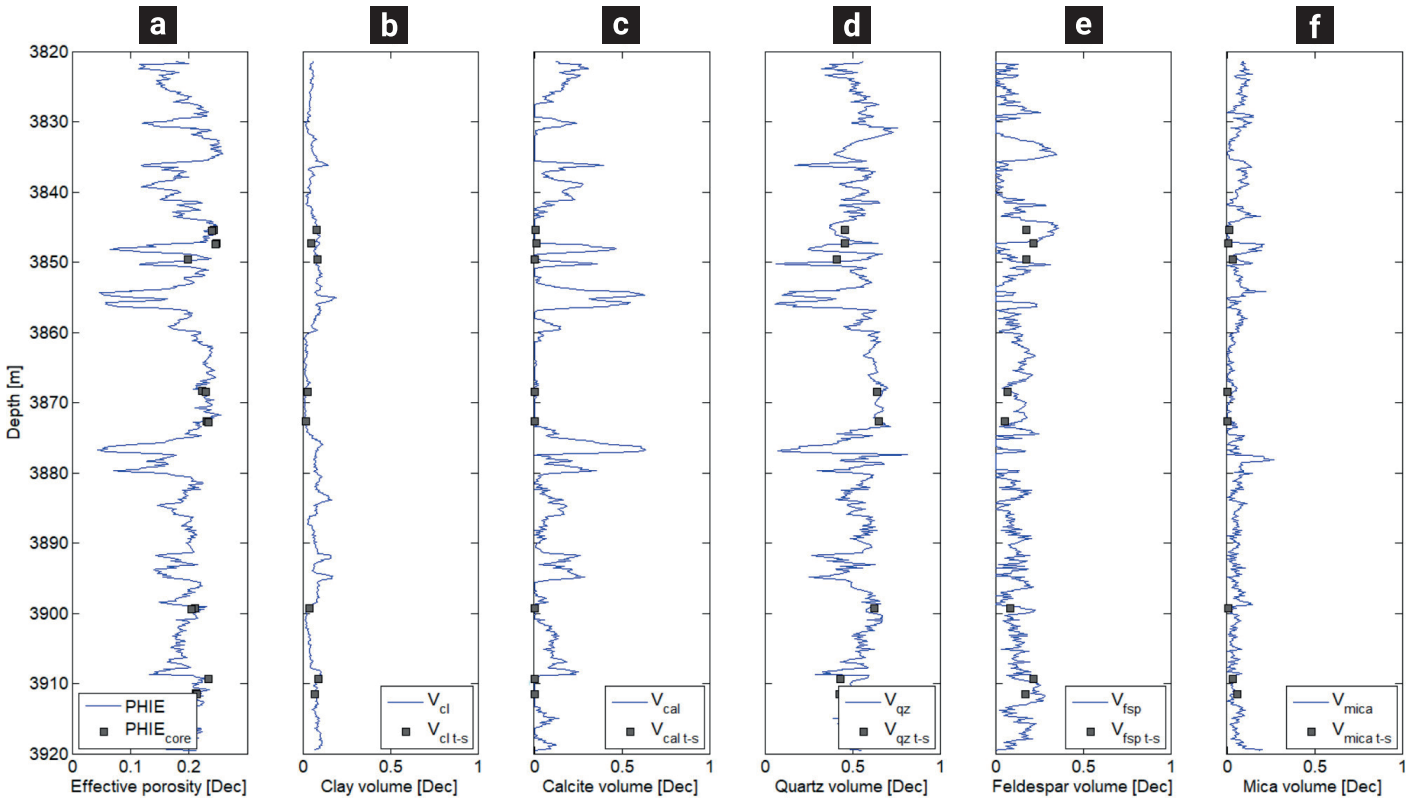

Figure 5. Calibrated results of a) estimated effective porosity (PHIE) and measured from core ($PHIE_{core}$), b) estimated clay volume (V_{cl}) and from thin section ($V_{cl\ t\text{-}s}$), c) estimated calcite volume and from thin section, d) estimated quartz volume (V_{qz}) and from thin section ($V_{qz\ t\text{-}s}$), and e) estimated feldspar volume (V_{fsp}) and from thin section ($V_{fsp\ t\text{-}s}$). The mineralogical volume fractions from thin section were obtained with the point-counting technique by Ringheim (1999).

Table 1. Mineral properties

Mineral	Density (g/cm^3)	K (GPa)	μ (GPa)	Reference
Calcite	2.71	74.8	30.6	Dandekar (1968)
Mixed feldspar	2.58*	54*	27*	
Mixed mica	2.98*	44*	16*	
Mixed clay	2.20*	9*	4*	
Quartz	2.65	39	33	Han *et al.*, (1986), Blangy (1992)

*Parameter estimated from mineralogy of thin section and Voigt-Reuss-Hill average.

Table 2. Fluid properties

Fluid	Water	Oil
Density (g/cm^3)	1.07*	0.73*
Bulk mudulus (GPa)	3.12*	0.72*

*Estimated using equation by Batzle and Wang (1992).

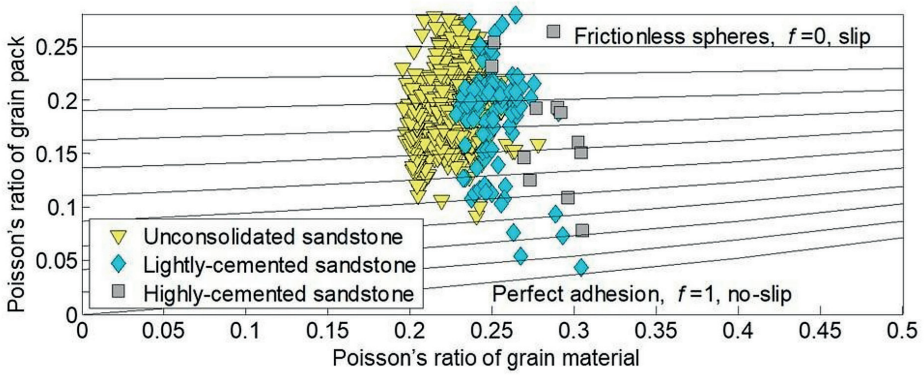

Figure 6. Estimation of friction coefficient in Hugin formation of the well 15/9–19A. The template is taken by Mavko *et al.*, (2009).

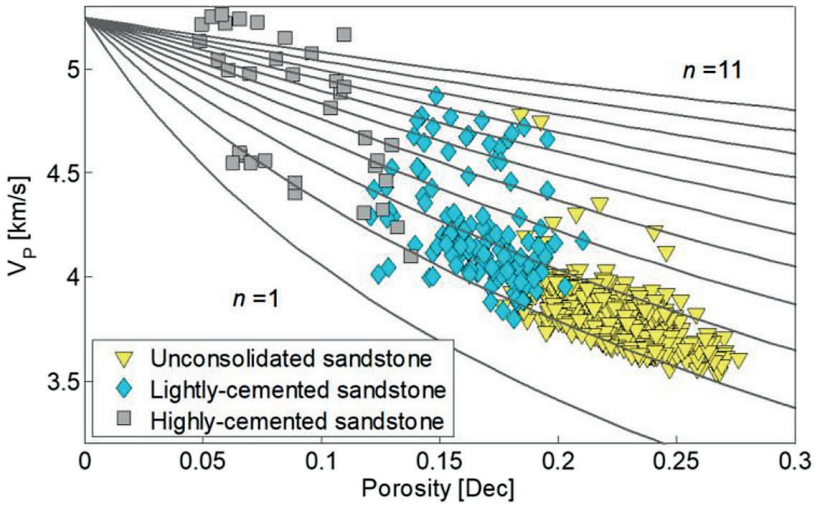

Figure 7. Rock physics diagnostics of the Hugin formation with the soft-sand model through compressional wave velocity versus porosity plot considering water saturation and reservoir conditions.

and 8, while the highly-cemented sandstone reaches values up to 11 (Figure 7). The Cement-Constant or Contact-Cement models could be chosen instead of the soft-sand model; nevertheless, the most significant amount of data corresponds to low coordination numbers. Dvorkin *et al.*, (2014) pointed out that the Hertz-Mindlin model could compute the dry elastic moduli instead of the Constant-Cement, but with a higher coordination number.

4.2.2 Differential Effective Medium Model (DEM) applied to Hugin formation

The Differential Effective Medium (DEM) model assumes inclusions embedding in a matrix host, which are added through an iterative homogenization process (Cleary *et al.*, 1980; Norris, 1985; Zimmerman, 1991).

Figure 8 shows the rock physics diagnostics in Hugin formation with DEM, where P- and S-wave velocities are plotted versus porosity. Note that the cross-plots present lines corresponding to the different aspect ratios (α) associated with the rock's microstructure. According to Figures 8a and b, the cross-plots of V_P and V_S indicate that the unconsolidated sandstone has an aspect ratio approximately between 0.1 and 0.3. Nevertheless, the sandstone with calcite cement has α values greater than 0.5 for V_P while for V_S the range is $0.05 < \alpha < 0.3$. Notice that the thin sections at 3854 and 3876 m (Figures 8c and d) show $\alpha\ (V_P) > 0.5$ while that $\alpha\ (V_S) \approx 0.05$. The thin section analysis indicates low porosity, cemented rock (Figure 8c) and microfractures (Figure 8d). This suggests that the pore structure is better determined from the aspect ratio from V_S diagnostics. However, notice that V_P diagnostics show high velocities associated with cemented

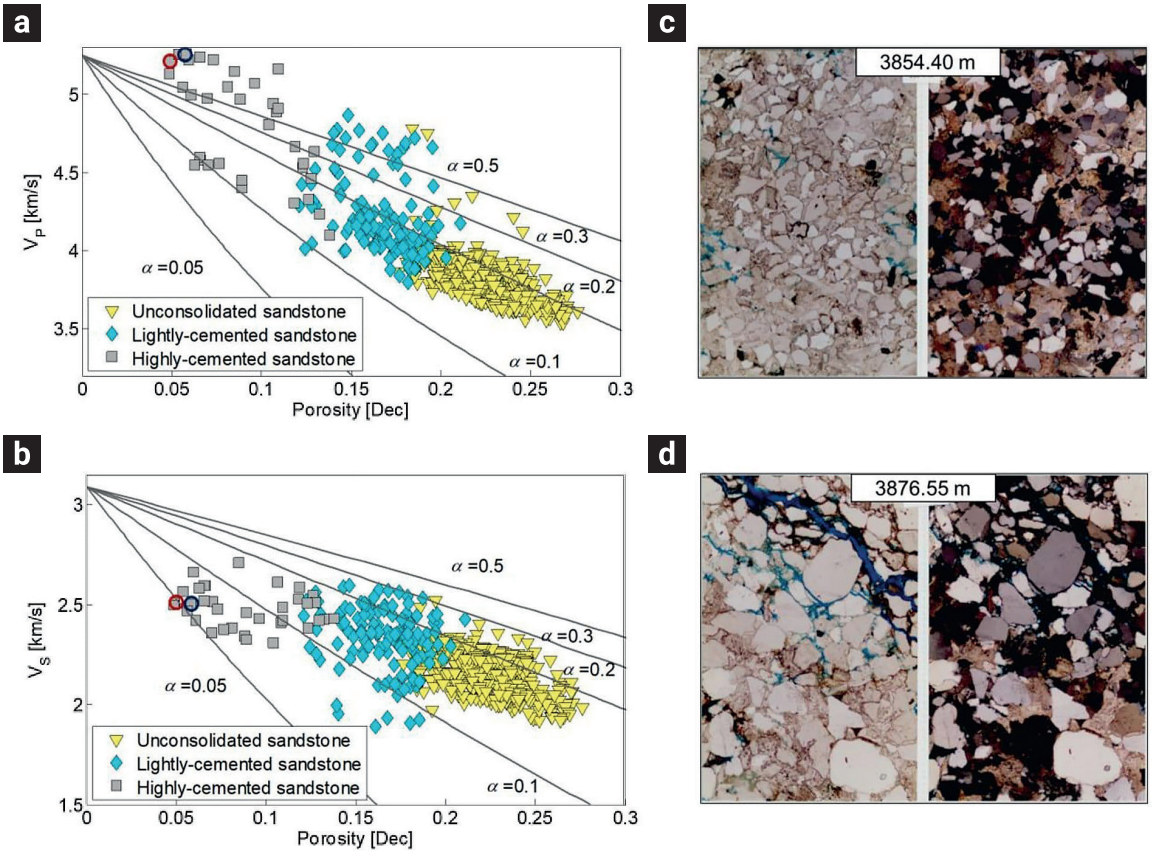

Figure 8. Rock physics diagnostics with Differential Effective Medium (DEM) model. a) Compressional wave velocity and b) shear wave velocity versus porosity considering different aspect ratios. These plots consider water saturation at reservoir conditions. c) Red and d) blue circles in velocity-porosity plots correspond to the thin sections at 3854.40 and 3876.55 m, respectively. The thin sections were taken by Statoil (1998a).

rock. A possible cause of the discrepancy in determining the aspect ratio between V_P and V_S could be related to the fact that V_P considers the fluid properties (Avseth, 2009). Another cause could be the shear wave splitting in an anisotropic medium.

Therefore, it was decided to apply an inversion scheme to determine the aspect ratio and K_{dry}. at each depth level. The objective function was taken by Li *et al.*, (2013) that considers V_P and V_S logs. It will be used in the next section.

4.3 Inversion scheme to obtain Z parameter and inverse quality factors

The inversion scheme provides obtaining the *Z* parameter in the squirt model (Figure 9). Rock and fluid properties are required in the model. The mixture of water and hydrocarbon was used to estimate the effective fluid modulus (K_{fl}). The matrix bulk modulus (K_o) was calculated with the Voigt-Reuss-Hill from mineralogy content and bulk elastic moduli of each mineral (Table 1). K_{dry} was estimated with aspect ratio inversion with the DEM model. $K_{dry\text{-}hip}$ was calculated from the soft sand model at high pressure and with K_{dry} of the DEM model until it matches with K_{dry} by the soft-sand model.

The next step is the prediction of P-($V_{P\text{-}ult}$) and S-wave ($V_{S\text{-}ult}$) velocities from core velocities ($V_{P\text{-}core}$,$V_{S\text{-}core}$) reported by Statoil (1998b) from a triaxial test at an ultrasonic frequency. $V_{P\text{-}core}$ and $V_{S\text{-}core}$ are 3.5% and 1.9% higher than the measured P-($V_{P\text{-}log}$) and S-wave ($V_{S\text{-}log}$) velocities from well logs, respectively (Figure 10).

It is important to point out that the frequency (f) selected in the methodology (Figure 2) is 10 kHz in the objective function (Eq. 7), which is within the range of the sonic tool's frequencies. The compressional and shear transit time logs are in the range of frequencies between 3 and 20 kHz (Tittman,1990). Ávila- Carrera *et al.*, (2010) gave more details of sonic tools in boreholes about propagation modes (Stoneley, pseudo-Rayleigh, and P waves) from numerical simulations compared with real well data.

The parameters K_o, K_{fl}, K_{dry}, $K_{dry\text{-}hip}$,$V_{P\text{-}log}$,$V_{S\text{-}log}$,$V_{P\text{-}ult}$ and $V_{S\text{-}ult}$ are inputs to apply the squirt flow model. The simulated annealing technique was used to solve the objective function (Eq. 7).

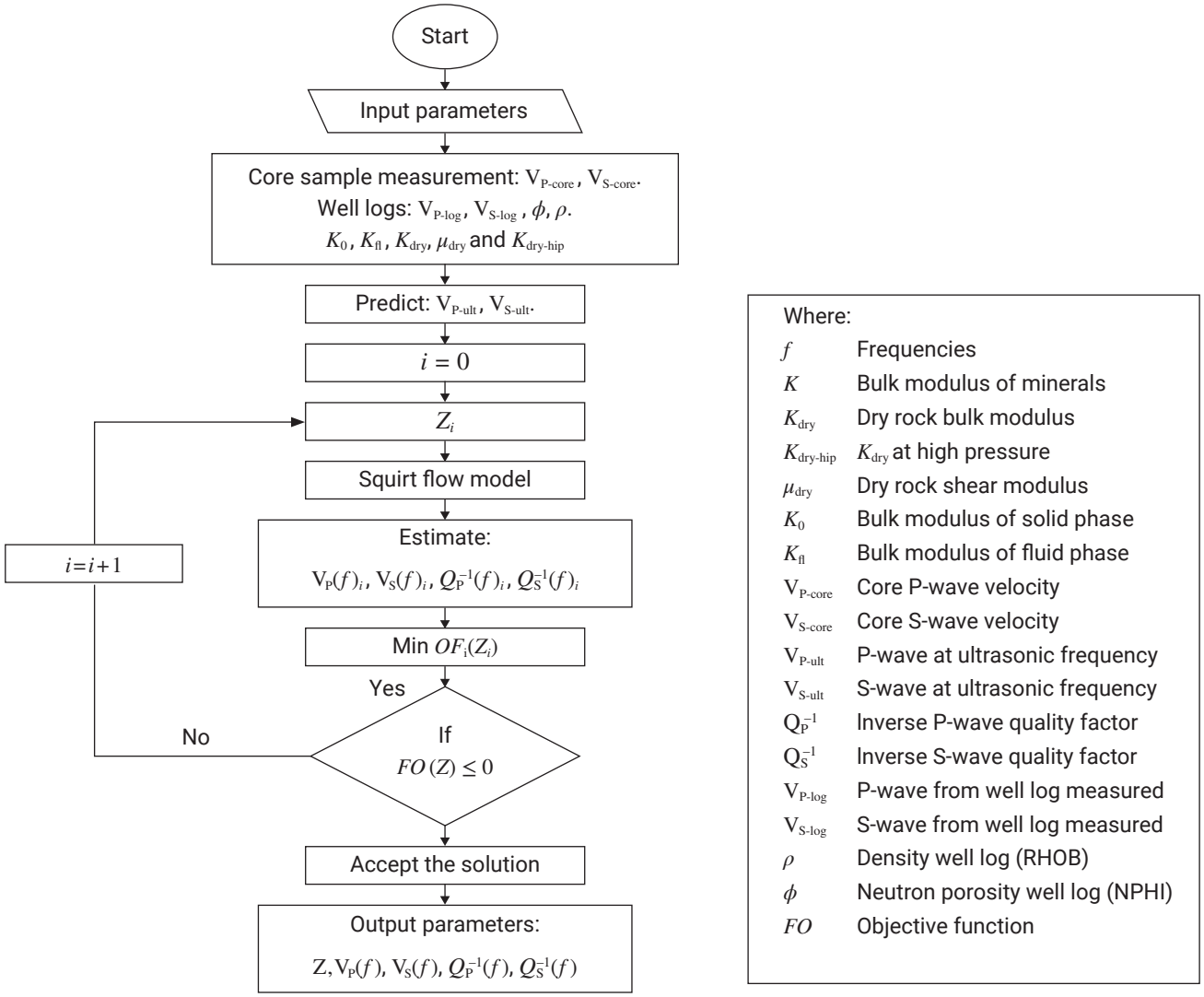

Figure 9. The inversion scheme to find parameters: Z, dispersion of velocities ($V_P(f)$, $V_S(f)$) and, inverse quality factors ($Q_P^{-1}(f)$, $Q_S^{-1}(f)$) by the squirt flow model.

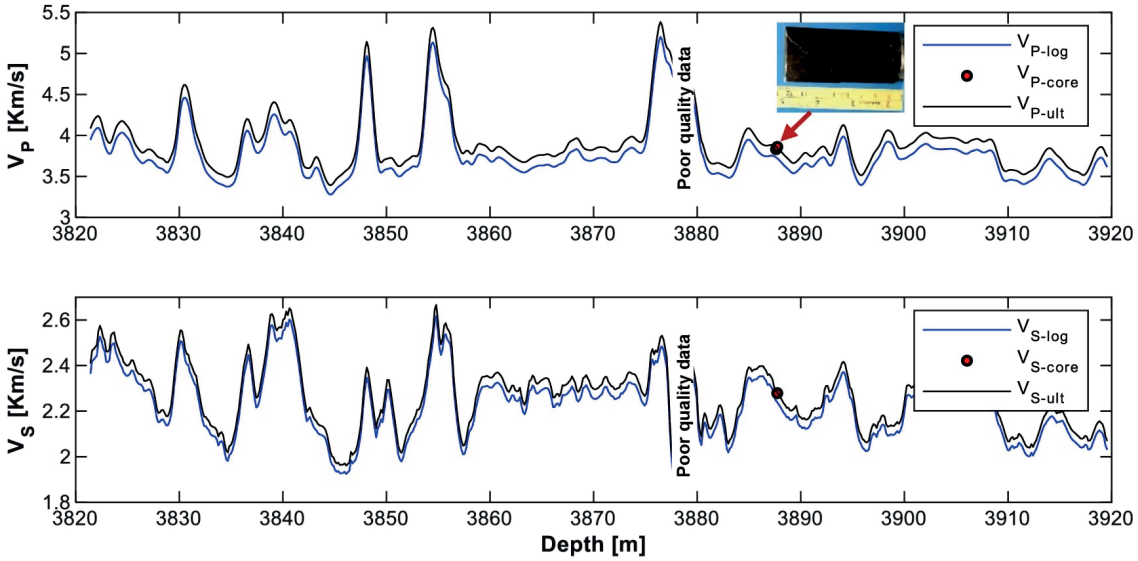

Figure 10. Prediction of P- ($V_{P\text{-ult}}$) and S-wave ($V_{S\text{-ult}}$) velocities from core velocities $V_{P\text{-core}}$ and $V_{S\text{-core}}$ reported by Statoil (1998b) at an ultrasonic frequency. $V_{P\text{-log}}$ and $V_{S\text{-log}}$ are the measured P- and S-wave velocities from well logs.

It starts with a value of Z, and the velocities and inverse quality factors are calculated. If the objective function is minimized, the solution is accepted. If not, the number of iterations is increased until the parameter Z that minimizes the objective function is found. This means that the error between the observed and estimated data is minimal. The inversion scheme allowed to predict the parameters: Z, $V_P(f)$, $V_S(f)$, $Q_P^{-1}(f)$ and $Q_S^{-1}(f)$ by matching observed sonic ($V_{P\text{-log}}$, $V_{S\text{-log}}$) and ultrasonic velocities ($V_{P\text{-ult}}$, $V_{S\text{-ult}}$) with the predicted velocties at 10 kHz and 0.5 MHz, correspondingly.

The Z parameter was determined by applying the inversion scheme at the core depth of 3887.7 m. The result was Z=0.0012063. Figure 11a shows a good correlation between the predicted dispersion of velocities and the measured velocities at sonic and ultrasonic frequencies. The predicted values of inverse quality factors for different frequencies are observed in Figure 11b.

The result of the inverted P-wave curves at 10 kHz ($V_{P\text{-log p}}$) and 0.5 MHz ($V_{P\text{-ult p}}$) fairly fit the measured P-wave velocity at sonic ($V_{P\text{-log}}$) and ultrasonic ($V_{P\text{-ult}}$) frequencies (Figures 12a and b). The inverted S-wave ($V_{S\text{-log p}}$,$V_{S\text{-ult p}}$) curves are different from the measured S-wave ($V_{S\text{-log}}$,$V_{S\text{-ult}}$) velocities in calcite zones at 3830, 3848, 3855, 3877, and 3899 m (Figures 12c and d). Figure 12e shows the results of Z parameter, which is higher in highly cemented sandstone with low porosity (ϕ<10%). The Z parameter decreases in the high oil saturation zone (3857-3875 m).

The inversion results show that the inverse quality factor at sonic frequency is lower than at ultrasonic frequency (see Figure 13a and b). The attenuation is high in the areas with partial saturation corresponding to unconsolidated sandstone and lightly cemented sandstone (3880-3919 m). The unconsolidated sandstone zone with high oil saturation ($85 < S_O > 95\%$) presents high values of inverse quality factor and low values of the Z parameter in the interval of 3857-3875 m. The zones corresponding to highly cemented sandstone saturated with high water saturation present low values of inverse quality factor and high values of Z. The ratio Q_S/Q_P is high in zones with highly cemented sandstone. On the other hand, Q_S/Q_P is low in unconsolidated sandstone (Figure 13).

4.4 Prediction of hydraulic permeability

Figure 14a shows the plot of Log Permeability by Timur (k_T) versus P-wave inverse quality factor (Q_{P-s}^{-1}) at a sonic frequency considering water saturation in color bar. When k_T is low, (Q_{P-s}^{-1}) is also low. The data trending is polynomial of high order. Log k_T versus Z parameter plot shows that if Z is low, then k_T is high, therefore the diffusivity of soft pore space is also high (Figure 14b). It means that in this type of medium, the attenuation is developed by incorporating the local pressure of pore fluid between soft and stiff pores.

The methodology (Figure 2) considers the correlation between Log Permeability by Timur (k_T) with: P-(Q_{P-s}^{-1}) and S (Q_{S-s}^{-1}) wave inverse quality factors at a sonic frequency, (Q_{P-s}^{-1}) and Z parameter, Q_{P-s}^{-1} and effective porosity (PHIE), and Z parameter and PHIE.

A fourth-degree polynomial regression was applied to perform the correlation Q_{P-s}^{-1} and Q_{S-s}^{-1}. The obtained correlation coefficient (R^2) was: 0.77. The next correlations Q_{P-s}^{-1} and Z

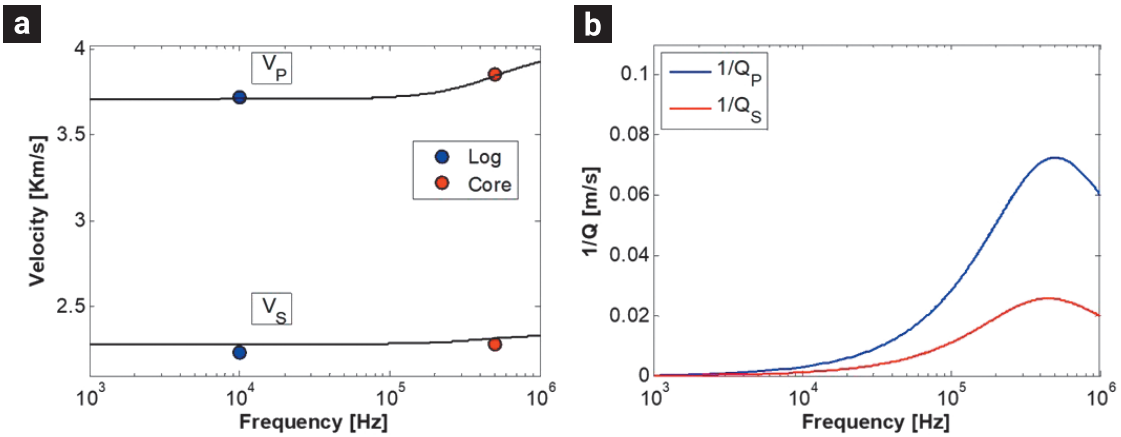

Figure 11. a) Prediction of P- and S-wave velocities versus frequencies from the squirt model where red and blue circles correspond to core velocities by Statoil (1998b) and velocities from well logs, respectively. b) Prediction of P- (Q_P^{-1}) and S-wave (Q_S^{-1}) inverse quality factors versus frequencies. The predictions were estimated from inversion by matching predicted to measured velocities at 3887.7 m, the result was Z=0.0012063.

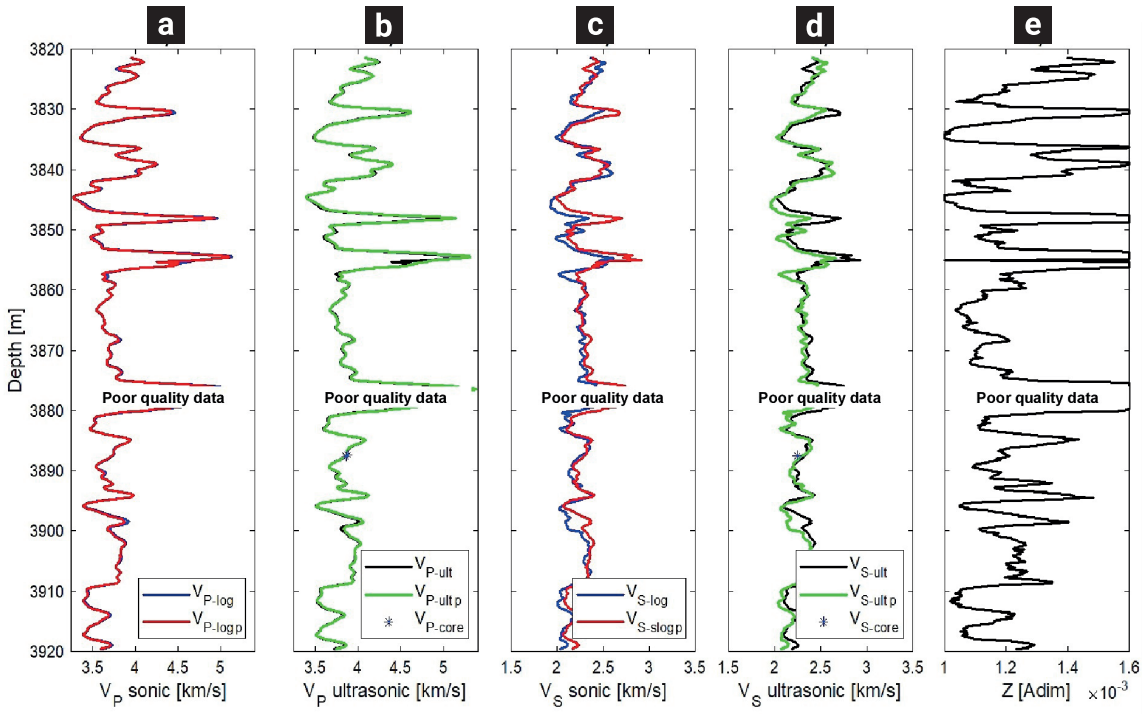

Figure 12. Velocity inversion results by the squirt flow model. a) P-wave sonic log ($V_{P\text{-log}}$) and predicted P-wave velocity ($V_{P\text{-log p}}$) at 10 kHz, b) ultrasonic P-wave velocity ($V_{P\text{-ult}}$) and predicted ultrasonic P-wave velocity ($V_{P\text{-ult p}}$) at 0.5 MHz, c) S-wave sonic log ($V_{S\text{-log}}$) and predicted S-wave velocity ($V_{S\text{-log p}}$) at 10 kHz, d) ultrasonic S-wave velocity ($V_{S\text{-ult}}$) and predicted ultrasonic S-wave velocity ($V_{S\text{-ult p}}$) at 0.5 MHz. Where $V_{P\text{-core}}$ and $V_{S\text{-core}}$ are core velocities reported by Statoil (1998b). e) Prediction of Z parameter.

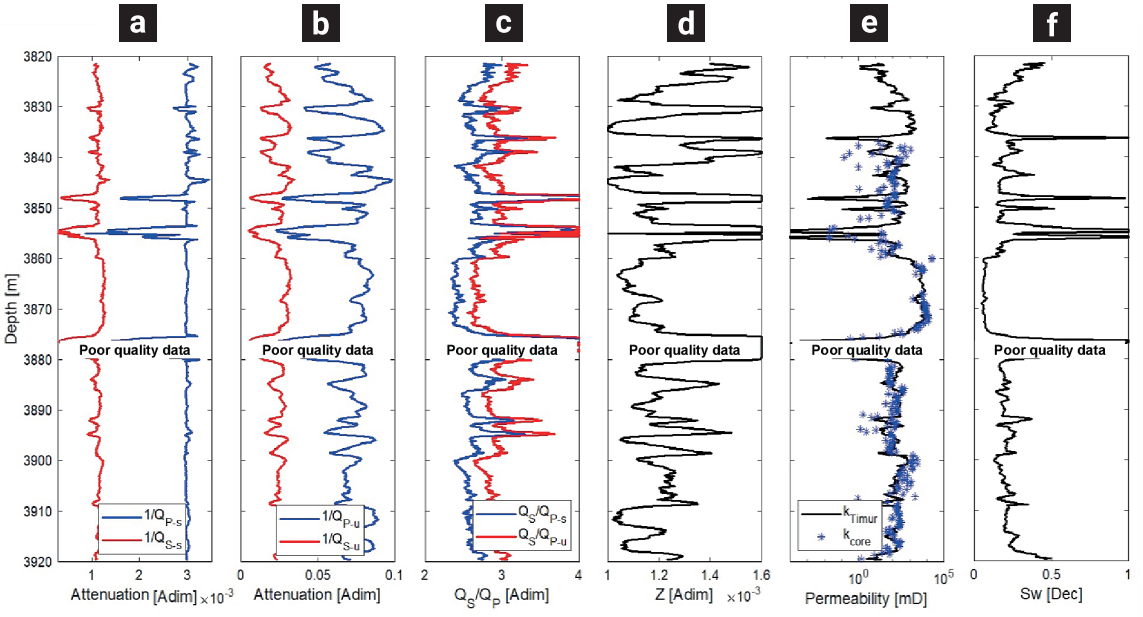

Figure 13. Attenuation results. Predicted P-(Q^{-1}_{P-s}) and S (Q^{-1}_{S-s}) wave inverse quality factors at a) sonic (10 kHz) and b) ultrasonic (0.5 MHz) frequencies. c) Ratio $Q_S/Q_{P\text{-s}}$ and $Q_S/Q_{P\text{-u}}$ at sonic and ultrasonic frequencies, respectively. d) Predicted Z parameter. e) Estimated permeability by Timur (k_T) and core permeability (k_{core}) reported by Byberg (1998). f) Water saturation (S_w).

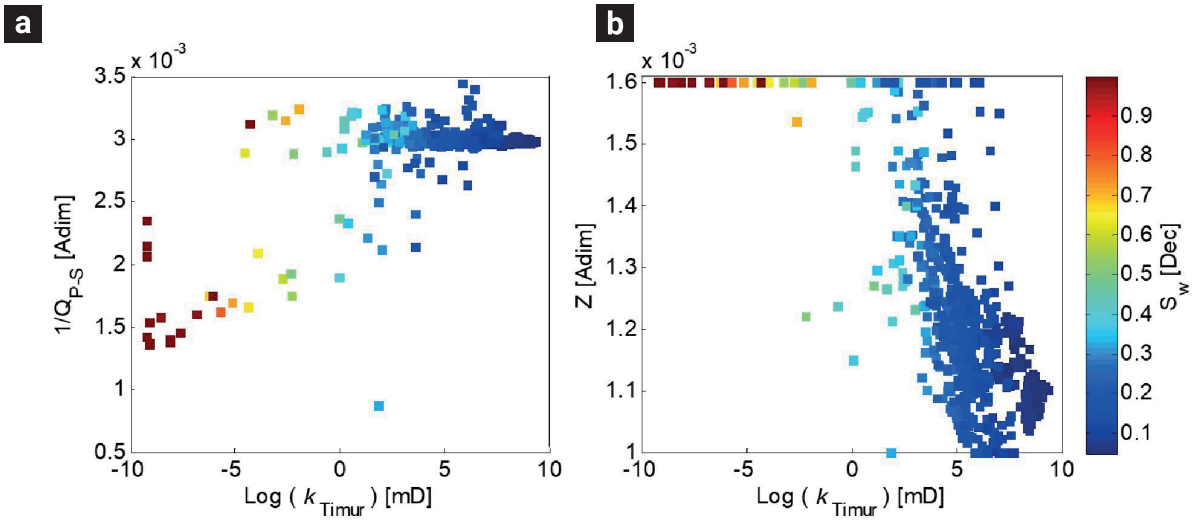

Figure14. Log Permeability by Timur (k_T) varying with: a) P-wave inverse quality factor (Q_{P-s}^{-1}) at a sonic frequency and b) Z parameter. The color bar indicates water saturation (S_w).

parameter, Q_{P-s}^{-1} and PHIE, Z and PHIE consider a third-degree polynomial regression where R^2 were 0.71, 0.9, and 0.89, respectively (Figure 15).

Figure 16 shows the results of the predicted hydraulic permeability from the correlation equations (Figure 15). Correlations with Q_{P-s}^{-1} and Q_{S-s}^{-1} display a good match concerning k_T and k_{core}, while Z and Q_{P-s}^{-1} does not show a good fit, although it presents certain tendencies with k_T and k_{core}. On the other hand, PHIE with Q_{P-s}^{-1} or Z parameter improve the prediction of hydraulic permeability.

5. Discussion

This work presents a methodology to predict hydraulic permeability based on the squirt's model. The measured velocities at sonic and ultrasonic frequencies were fit with the predicted dispersion velocity to find the inverse quality factors and the Z parameter from a global inversion in the Hugin formation. The predicted attenuations and the Z parameter were used to estimate hydraulic permeability. According to the results, the values of inverse quality factors are high, and the Z values are low in zones which present high values of porosity ($20\% < \phi > 30\%$), permeability ($200\,mD < k$), and oil saturation ($85\% < S_o > 95\%$), that corresponds to unconsolidated sandstone and lightly cemented sandstone.

Henceforth, the predicted model was used to correlate hydraulic permeability with inverse quality factors, Z parameter, and effective porosity. These correlations showed good predictions and were validated with core data. It is suggested that predictive modeling algorithms such as decision trees, nearest neighbor, logistic regression, and neural networks, which require training time and are more complex (Abbot, 2014), could improve the k prediction.

There are few core velocity data to obtain a curve of velocity at ultrasonic frequency. It must be carefully analyzed since other core velocity values were removed because these values were lower than the velocity logs (at a sonic frequency), which means that cores were not preserved at pressure and temperature conditions.

On the other side, this methodology could be used in other models that consider the mesoscopic scale (White, 1975), double porosity and double permeability (Ba *et al.*, 2014), squirt flow model that considers pores and cracks with different orientations (Chapman *et al.*, 2002) or anisotropic squirt.

This work is relevant because the squirt flow model can be used to predict permeability from measured velocity data at different frequencies. In this case, sonic and ultrasonic velocity data are used. However, it could be applied to seismic data and sonic data. It will support using seismic data to predict hydraulic permeability since seismic data includes a lot of information. In comparison to this methodology, the limitations of wireline formation testers are that they provide measurements by layer thickness, and data are affected by skin and tool storage (Ayan *et al.*, 2021). Soleimani *et al.*, (2018) used Stoneley wave to predict permeability. However, on occasions, this wave is not measured in wells, and IMF is a parameter needed to obtain permeability, and it's not clear how it is determined. Equations such as Timur, Willye and Rose, Kozeny, and Carman (Tiab and Donaldson, 2004) require irreducible water saturation, which is only obtained by the NMR log, and not all wells have this well log. The proposed methodology could be applied to predict

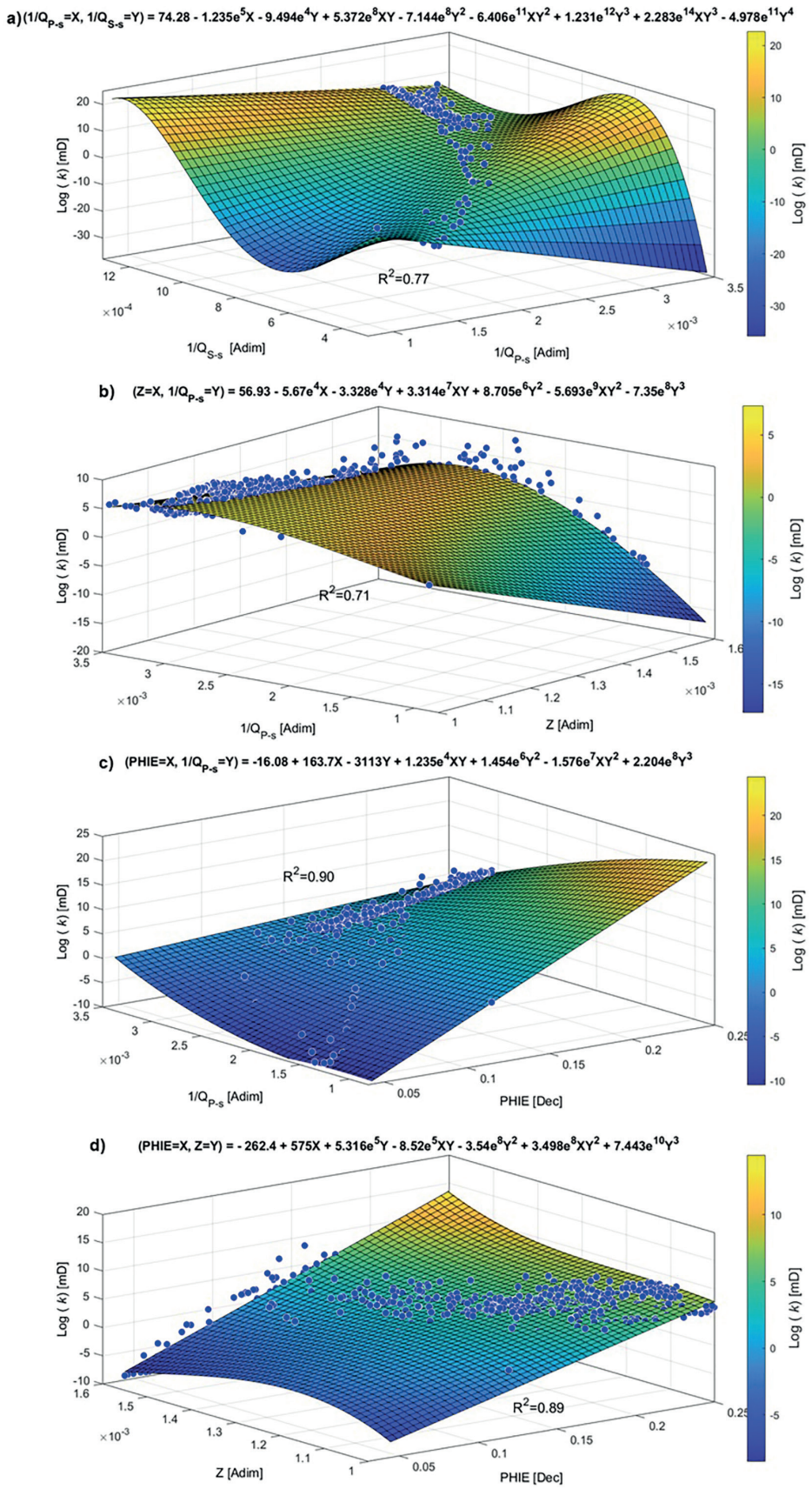

Figure 15. Correlation of Log Permeability by Timur (k_T) with: a) P-(Q_{P-s}^{-1}) and S (Q_{S-s}^{-1}) wave inverse quality factors at a sonic frequency, b) Q_{P-s}^{-1} and Z parameter, c) Q_{P-s}^{-1} and effective porosity (PHIE), and d) Z parameter and PHIE.

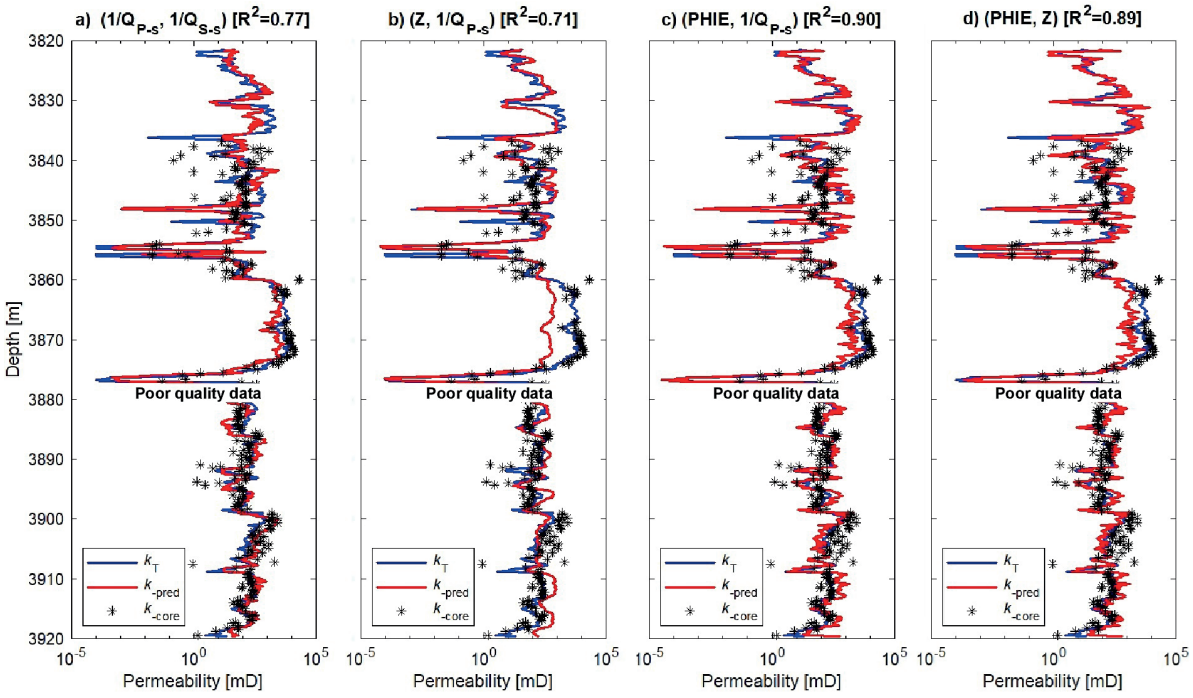

Figure 16. Predicted hydraulic permeability from a) P-(Q_{P-s}^{-1}) and S (Q_{S-s}^{-1}) wave inverse quality factors at a sonic frequency, b) Z parameter and Q_{P-s}^{-1}, c) Effective porosity (PHIE) and Q_{P-s}^{-1}, and d) PHIE and Z parameter compared to permeability by Timur (k_T) and core permeability (k_{core}) reported by Byberg (1998).

hydraulic permeability from inverse quality factors and other properties in wells at sonic and considering the information of the seismic cube.

6. Conclusions

A four-stage methodology based on the squirt flow model was proposed to predict hydraulic permeability. The first stage includes the petrophysical evaluation, which was validated with core properties and thin sections. The next stage is the rock physics diagnostics that was applied to identify the rock's microstructure, and three facies were recognized from the velocity-porosity relationship. The inputs to apply the squirt flow model are estimated in the first and second stages. The third stage considers the inversion scheme to predict P- and S-wave velocities, inverse quality factors at different frequencies, and the Z parameter from minimizing an objective function. The last stage consisted of the k prediction from correlation functions.

The squirt flow model, a key tool in this research, approximates the attenuation due to an induced pressure between the solid matrix and fluid during wave propagation. This model is particularly effective in understanding the behavior of unconsolidated sandstone and lightly cemented sandstone with high oil saturation, which presents high values of inverse quality factors and low values of the Z parameter, indicating high permeability and diffusivity of soft pore space. Conversely, the highly-cemented sandstone with high water saturation reaches low values of inverse quality factors with high Z values, suggesting low permeability and diffusivity of soft pore space. This understanding is crucial as it is related to porosity, with unconsolidated sandstone and lightly cemented sandstone having more pore space to develop cross-flow between soft and stiff pores.

The permeability by Timur (k_T) correlated with inverse quality factors and Z parameter. The correlations with effective porosity showed a better match with the hydraulic permeability from the core data.

The correlation functions could be applied in future works to predict hydraulic permeability in neighboring wells. This work could be enhanced by leveraging other tools, such as another inversion approach, multiple correlation coefficients, or a machine learning scheme. Instead of using the inverse quality factors at a frequency to estimate hydraulic permeability, the attenuation could be explored over the full frequency band with the known Z parameter by the inversion approach. These potential

improvements could facilitate research and development in the field of hydraulic permeability prediction from seismic data and sonic logs.

7. Acknowledgment

The authors highly appreciate the Equinor and the Volve license partners for permitting the use of their available data.

8. Appendix A

The expressions of the squirt flow model are described below. K_{msd} is the bulk modulus of the dry modified solid by Dvorkin *et al.*, (1995):

$$K_{msd} = \left[\frac{1}{K_0} - \frac{1}{K_{dry\text{-}hip}} + \frac{1}{K_{dry}} \right]^{-1}, \qquad (A1)$$

The $\frac{dP}{d\sigma}$ describe the ratio between the increments of pore pressure (dP) and confining stress increment:

$$\frac{dP}{d\sigma} = -\left[\alpha_0 \left(1 + \frac{\phi K_{dry}}{\alpha_0^2 F_0} \right) \right]^{-1}, \qquad (A2)$$

where α_0 is the Biot-Willis coefficient and ϕ is the porosity. F_0 is given for:

$$F_0 = \left[\frac{1}{K_{fl}} + \frac{1}{\phi Q_0} \right]^{-1} \qquad (A3)$$

with:

$$Q_0 = \frac{K_0}{\alpha_0 - \phi}. \qquad (A4)$$

K_{ms} is the bulk modulus of the saturated modified solid:

$$K_{ms} = \left[\frac{K_{msd} + \alpha K_0 \left[1 - f(\xi) \right]}{1 + \alpha f(\xi) \frac{dP}{d\sigma}} \right], \qquad (A5)$$

where:

$$\alpha = 1 - \frac{K_{msd}}{K_0}, \quad f(\xi) = \frac{2J_1(\xi)}{\xi J_0(\xi)}, \quad \xi = Z\sqrt{i\omega} \qquad (A6)$$

J_o and J_1 are the Bessel function of zero and first order, correspondingly. ω is the angular frequency.

In Eq. 1 is needed the bulk modulus of the modified frame which is given by:

$$K_m = \left[\frac{1}{K_{ms}} + \frac{1}{K_{dry\text{-}hip}} - \frac{1}{K_0} \right]^{-1} \qquad (A7)$$

To estimate μ_m in Eq. 2, K_{md} is obtained from:

$$K_{md} = \left[\frac{1}{\bar{K}_{ms}} + \frac{1}{K_{dry\text{-}hip}} - \frac{1}{K_0} \right]^{-1}, \qquad (A8)$$

where : $\bar{K}_{ms}=K_{msd}+\alpha K_0\,[1-f(\xi)]$.

References

Abbot, D. (2014). *Applied Predictive Analytics: Principles and Techniques for the Professional Data Analyst*. John Wiley & Sons, Inc., Indianapolis, Indiana.

Akbar, N., Dvorkin, J., Nur, A. (1993). Relating P-wave attenuation to permeability. *Geophysics* 58(1), 20-29. doi: **https://doi.org/10.1190/1.1443348**

Ávila-Carrera, R., Spurlin, H. J., Valle-Molina, C. (2010). Simulating elastic wave propagation in boreholes: Fundamentals of seismic response and quantitative interpretation of well log data. *Geofísica Internacional*, 50(1), 57-76. doi: **https://doi.org/10.22201/igeof.00167169p.2011.50.1.122**

Avseth, P., Jorstad, A., Van, W. A-J., Mavko, G. (2009). Rock physics estimation of cement volume, sorting, and net-to-gross in North Sea sandstones. *The Leading Edge*, 28, 98-108. doi: **https://doi.org/10.1190/1.3064154.**

Ayan, C., Hafez, H., Hurst, S., Kuchuk, F., O'Callaghan, A., Peffer, J., Pop, J., Zeybek, M. (2001). Characterization Permeability with Formation Tester. *Oilfield Review*, 13(3), 2-23.

Ba, J., Yuan, Z., Carcione, J. M., Guo, Y., Zhang, L., Sun, W. (2015). *Wave propagation and attenuation in heterogeneous reservoir rocks*. En A. Ba, J., Du, Qizhen., Carcione, José M., Zhang, H., Müller, T. M. (Eds), Seismic Exploration of Hydrocarbons in Heterogeneous

Reservoirs. (pp. 9-43). Elsevier.

Batzle, M., Wang Z. (1992). Seismic properties of pore fluids. *Geophysics*, 57, 1396-1408. doi: **https://doi.org/10.1190/1.1443207.**

Blangy, J. D. (1992). *Integrated seismic lithologic interpretation: The petrophysical basis*. [PhD. Dissertation]. Stanford University.

Byberg, O. (1998). *Conventional Core Analysis, Well 15/9-19A*, (Report 10177-97). Norway.

Chapman, M., Zatsepin, S. V., Crampin, S. (2002). Derivation of a microstructural poroelasticity model. *Geophysical Journal International*, 151(2), 427-451. doi: **https://doi.org/10.1046/j.1365-246X.2002.01769.x**

Cleary, M.P., Lee, S.-M., Chen, I.-W. (1980). Self-Consistent Techniques for Heterogeneous Media. *Journal of the Engineering Mechanics Division*. 106(5), 861-887. doi: **https://doi.org/10.1061/JMCEA3.0002643**

Dandekar, D. P. (1968). Pressure Dependence of the Elastic Constants of Calcite. *Physical Review Journal Archive*, 172, 873-877. doi: **https://doi.org/10.1103/PhysRev.172.873**

Dvorkin J., Gutierrez M. A., Grana D. (2014). *Seismic reflections of rock properties*, (1 ed.) Cambridge University Press, United Kingdom.

Dvorkin, J., Mavko, G., Nur, A. (1995). Squirt flow in fully saturated rocks. *Geophysics*, 60(1), 97-107. doi: **https://doi.org/10.1190/1.1443767**

Dvorkin, J., Nolen-Hoeksema, R., Nur, A. (1994). The squirt-flow mechanism: Macroscopic description. *Geophysics*, 59(3), 336-490. doi: **https://doi.org/10.1190/1.1443605**

Dvorkin, J., Nur, A. (1993). Dynamic poroelasticity: A unified model with the squirt and the Biot mechanism. *Geophysics*, 58, 524-533. doi: **https://doi.org/10.1190/1.1443435**

Dvorkin, J., Nur, A. (1996). Elasticity of high-porosity sandstone: Theory for two North Sea data sets. *Geophysics*, 61, 1363-1370. doi: **https://doi.org/10.1190/1.1444059**

Gassmann, F. (1951). Über die Elastizität poröser Medien.Vierteljahrsschrift der Naturforschenden Gesellschaft in Zürich 96, 1-23.

Han, D.-H., Nur, A., Morgan, D. (1986). Effects of porosity and clay content on wave velocities in sandstones. *Geophysics*, 51, 2093-2107. doi: **https://doi.org/10.1190/1.1442062**

Li, H.-B., Zhang, J.-J., Yao, F.-C. (2013). Inversion of effective pore aspect ratios for porous rock and applications. *Chinese Journal of Geophysics*, 56(1), 43-51. doi: **https://doi.org/10.1002/cjg2.20004**

Lunde, B. (2013). *Diagenesis and Reservoir Quality of the Hugin Formation Sandstones in the North Sea, a Petrographical Approach*. [Master thesis]. Norwegian University of Science and Technology.

Mavko, G., Mukerji, T., Dvorkin, J. (2009). *The Rock Physics Handbook. Tools for Seismic Analysis of Porous Media.* (2 Ed.) Cambridge University Press, Cambridge.

Mindlin, R. D. (1949). Compliance of Elastic Bodies in Contact. Journal of Applied Mechanics 16(3), 259-268. doi: **https://doi.org/10.1115/1.4009973**

Müller, T., Gurevich, B., Lebedev, M. (2010). Seismic wave attenuation and dispersion resulting from wave-induced flow in porous rocks-A review. *Geophysics*, 75(5), 75A147-75A164. doi: **https://doi.org/10.1190/1.3463417**

Nolen-Hoeksema, R. (2014). Defining and Determining Permeability. *Oilfield Review*, 26(3), 63-64.

Norris A.N. (1985). A differential scheme for the effective moduli of composites. *Mechanics of Materials* 4(1), 1-16. doi: **https://doi.org/10.1016/0167-6636(85)90002-X**

Østby, J. M, Frafjord, D., Tveit, L. (1998). *Final Well Report well 15/9-19A*, (ReportPL 046). Norway.

Palmer, I. D., Traviolia, M. L. (1980). Attenuation by squirt flow in undersaturated gas sand. *Geophysics* 45(12), 1780-1792. doi: **https://doi.org/10.1190/1.1441065**

Pride, S. R., Berryman, J. G., Harris, J. M. (2004). Seismic attenuation due to wave-induced flow. *Journal of Geophysical Research Solid Earth*,109(B1), 1-19. doi: **https://doi.org/10.1029/2003JB002639**

Ringheim, M. (1999). *Special Core Analysis, Sleipner, Well 15/9-19A*, (Report30131/24-99). Norway.

Schlumberger (2014). *DSI Dipole Shear Sonic Imager*. [Dipole sonic imager]. Schlumberger.

Shapiro, S. A., Müller, T. M. (1999). Seismic signatures of permeability in heterogeneous porous media. *Geophysics*, 64, 99-103. doi: **https://doi.org/10.1190/1.1444536**

Soleimani, B., Moradi, M., Ghabeishavi, A. (2018). Stoneley Wave Predicted Permeability and Electrofacies Correlation in the Bangestan Reservoir, Mansouri Oilfield, SW Iran. *Geofísica Internacional*, 57(2), 107-120. **https://doi.org/10.22201/igeof.00167169p.2018.57.2.2040**

Statoil (1998a). *Micro photographs thin sections, well: 15/9-19A*, p. 90

Statoil (1998b). *Rock Mechanical Testing, Triaxial tests on sandstone, well 15/9-19A*, p. 60.

Tiab, D., Donaldson, E.C. (2004). Petrophysics: *Theory and Practice of Measuring Reservoir Rock and Fluid Transport Properties*, (2 Ed.). Elsevier.

Tittman, J. (1990). Shear Wave Logging with Dipoles. *Oilfield Review* 2, 9-12.

Tjomsland, T. (1998). *Recombination and PVT analysis core flooding study, well 15/9-19A*, (Report STAT617), p. 43. Norway.

Vollset, J., Doré A. G. (1984). A revised Triassic and Jurassic lithostratigraphic nomenclature for the Norwegian North Sea. *NPD-Bulletin*, 3, 1-53.

White, J. E. (1975). Computed seismic speeds and attenuation in rocks with partial gas saturation. *Geophysics* 40(2), 224-232. doi: **https://doi.org/10.1190/1.1440520**

Zimmerman, R.W. (1991). Elastic moduli of a solid containing spherical inclusions. *Mechanics of Materials,*12(1), 17-24. doi: **https://doi.org/10.1016/0167-6636(91)90049-6**